

AD _____

CONTRACT NUMBER DAMD17-93-C-3071

TITLE: Early Detection of Breast Cancer and Recurrence Using
Near Infrared Time Resolved Spectrophotometry

PRINCIPAL INVESTIGATOR: Lawrence Solin, M.D., Ph.D.

CONTRACTING ORGANIZATION: University of Pennsylvania
Philadelphia, Pennsylvania 19104

REPORT DATE: March 1997

TYPE OF REPORT: Final

PREPARED FOR: Commander
U.S. Army Medical Research and Materiel Command
Fort Detrick, Frederick, Maryland 21702-5012

DISTRIBUTION STATEMENT: Approved for public release;
distribution unlimited

The views, opinions and/or findings contained in this report are those of the author(s) and should not be construed as an official Department of the Army position, policy or decision unless so designated by other documentation.

DTIC QUALITY INSPECTED 3

19970711 114

REPORT DOCUMENTATION PAGE			Form Approved OMB No. 0704-0188	
Public reporting burden for this collection of information is estimated to average 1 hour per response, including the time for reviewing instructions, searching existing data sources, gathering and maintaining the data needed, and completing and reviewing the collection of information. Send comments regarding this burden estimate or any other aspect of this collection of information, including suggestions for reducing this burden, to Washington Headquarters Services, Directorate for Information Operations and Reports, 1215 Jefferson Davis Highway, Suite 1204, Arlington, VA 22202-4302, and to the Office of Management and Budget, Paperwork Reduction Project (0704-0188), Washington, DC 20503.				
1. AGENCY USE ONLY (Leave blank)	2. REPORT DATE March 1997	3. REPORT TYPE AND DATES COVERED Final (15 Mar 93 - 14 Feb 97)		
4. TITLE AND SUBTITLE Early Detection of Breast Cancer and Recurrence Using Near Infrared Time Resolved Spectrophotometry		5. FUNDING NUMBERS DAMD17-93-C-3071		
6. AUTHOR(S) Lawrence Solin, M.D.				
7. PERFORMING ORGANIZATION NAME(S) AND ADDRESS(ES) University of Pennsylvania Philadelphia, Pennsylvania 19104		8. PERFORMING ORGANIZATION REPORT NUMBER		
9. SPONSORING/MONITORING AGENCY NAME(S) AND ADDRESS(ES) Commander U.S. Army Medical Research and Materiel Command Fort Detrick, Frederick, MD 21702-5012		10. SPONSORING/MONITORING AGENCY REPORT NUMBER		
11. SUPPLEMENTARY NOTES				
12a. DISTRIBUTION / AVAILABILITY STATEMENT Approved for public release; distribution unlimited		12b. DISTRIBUTION CODE		
13. ABSTRACT (Maximum 200) The techniques are employed to measure the optical absorption and scattering factors of breast tissue: 1) A pulse time device in which light at a low power (50 mW) laser diode) is employed. The time delay in light propagation from the input to output of fiber optic couplers is related to the scattering factor (μ_s') and the rate of decay of emerging photons is related to the absorption factor (μ_a). 2) Phase modulation, which is more convenient and rapid, measures the phase shift of a high frequency oscillating light of approximately the same power and wavelength used in the pulse time method. Here, there is direct reading of the time delay which is characteristic of the scattering and absorption of tissue. Contrast agents may be used to increase the tumor detection sensitivity. For example, the absorption of porphyrins at 620 nm and indocyanine green at 806 nm, afford possibilities to follow the time course of tumor uptake of optical contrast agents. Histopathological confirmation of diagnosis will be obtained and correlated with the optical and MRI results. Both the imaging and optical data obtained from this proposed project will facilitate research on using the optical properties of breast tissue to screen for early stage cancer. The task requirements are believed to have been fully met, 93 tumor bearing breasts, 15 imaged, 54 μ_s , μ_s' determinations, 23 O_2 saturation, 1 with IV indocardiogreen (1500 measurements).				
14. SUBJECT TERMS Breast Cancer			15. NUMBER OF PAGES 36	
			16. PRICE CODE	
17. SECURITY CLASSIFICATION OF REPORT Unclassified	18. SECURITY CLASSIFICATION OF THIS PAGE Unclassified	19. SECURITY CLASSIFICATION OF ABSTRACT Unclassified	20. LIMITATION OF ABSTRACT Unlimited	

FOREWORD

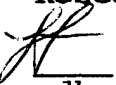
Opinions, interpretations, conclusions and recommendations are those of the author and are not necessarily endorsed by the US Army.

N/A Where copyrighted material is quoted, permission has been obtained to use such material.

N/A Where material from documents designated for limited distribution is quoted, permission has been obtained to use the material.

N/A Citations of commercial organizations and trade names in this report do not constitute an official Department of Army endorsement or approval of the products or services of these organizations.

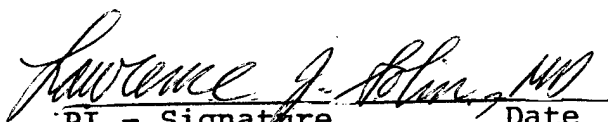
N/A In conducting research using animals, the investigator(s) adhered to the "Guide for the Care and Use of Laboratory Animals," prepared by the Committee on Care and Use of Laboratory Animals of the Institute of Laboratory Resources, National Research Council (NIH Publication No. 86-23, Revised 1985).

 For the protection of human subjects, the investigator(s) adhered to policies of applicable Federal Law 45 CFR 46.

N/A In conducting research utilizing recombinant DNA technology, the investigator(s) adhered to current guidelines promulgated by the National Institutes of Health.

N/A In the conduct of research utilizing recombinant DNA, the investigator(s) adhered to the NIH Guidelines for Research Involving Recombinant DNA Molecules.

N/A In the conduct of research involving hazardous organisms, the investigator(s) adhered to the CDC-NIH Guide for Biosafety in Microbiological and Biomedical Laboratories.


PI - Signature Date

1/24/97

DDO QUALITY INSPECTED 8

TABLE OF CONTENTS

Final Report

Early Detection of Breast Cancer & Recurrence Using Near Infrared Time Resolved Spectrophotometry

Lawrence Solin, M.D., Principal Investigator

	<u>Page Numbers</u>
Front Cover.....	1
SF298.....	2
Foreword.....	3
Table of Contents.....	4
Introduction	5
Body (Sections 1 through5).....	5-22
Conclusions.....	22-23
References.....	23
Appendix	

Final Report

Contract: US Army Med. R&D Command DAMD 17-93-C3071

Title: "Early Detection Breast Cancer and Recurrence using Near Infrared Time Resolved Spectrophotometry"

Principal Investigator: Lawrence Solin, MD

Co-Investigators: Britton Chance, Ph.D.
Susan Orel, MD

INTRODUCTION - Tasks Undertaken

In the first and second years of contract support, we have followed the assigned tasks on the imaging capability and tumor characterization in human breasts using TRS (time resolved spectroscopy) for 1500 measurements. We have computed optical characterization; i.e., μ_a (absorption) and μ_s' (scattering) measurements for 20, 34, and 6 patients in the first, second and third years, respectively. The statistics of the 60 patients with various stages of tumors are available and compared to 17 healthy normal controls. For the imaging capability, we have shown that with the current technologies and the current limitations, we can detect objects of ~ 1 cm. Longer times and transmission studies will improve the resolution.

In the past year (year 3) we have studied intensively novel modalities. The specified tasks required 360 studies. 1) TRS or PMS (phase modulation spectroscopy) can be used to identify oxygenation and scattering coefficient of tumors. 2) TRS may not be the best method to provide imaging mainly because of time requirements. Thus, we concluded that the TRS is perhaps more suitable for accurate measurements of the optical characterization, such as hemoglobin oxygenation in the tumor and scattering coefficients. In addition, our interests in the optical imaging now include the application of PMS and CWS (continuous wave spectroscopy).

In the following sections, we report on various tasks as follows:

- 1) Optical breast imaging using TRS;
- 2) TRS Study of optical characterization;
- 3) Present and future plans for the TRS system for optical characterization in tumor bearing breasts;
- 4) CWS breast imaging with contrast agent;
- 5) Imaging using the frequency domain method.

1. OPTICAL BREAST IMAGING USING TRS (Years 1 and 2)

1.1. Introduction

Despite the long history of the optical imaging technology, it has not been commonly used for breast cancer detection. Photon diffusion into the tissue makes a shadow of the object too obscure to use for imaging. The shadow imaging with continuous light (diaphanography) has been used in Asia, where average breast size is relatively smaller, but the shadow technique does not allow real imaging. Today, with new technologies, such as the time gated technique (1), more diffusive photons are eliminated and therefore better images can be obtained. We have studied the ability of the time gated optical technique to human breast cancer.

We have chosen to develop the time gated optical technique for breast cancer detection for the following reasons. First, the breast tissue consists of a relatively low scattering media, namely fat, whose scattering coefficient is as low as 3 cm^{-1} . Second, the breast is located on the surface of the

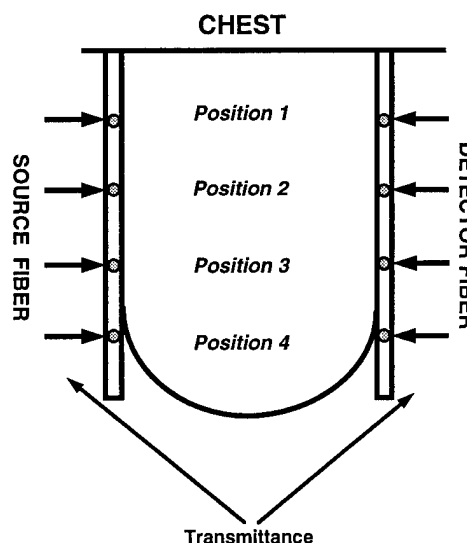
body and is accessible to the optical instruments. Thirdly, the time gated technique will allow selection of photons which have not diffused extensively (the extensively diffused photons are the ones which create obscure images). We selected 15% of total photons, which diffused relatively less and arrived earlier than 85% of rest of photons. We emphasize not only possible improvement of sensitivity of detection by this time gated technique, but also high specificity of cancer detection by functional imaging. It creates an oxygen image, a blood volume image and a scattering image, and therefore can be helpful in interpreting the cell function of lesions. Preliminary studies using TRS for characterizing tumors in the breast have been published elsewhere (2).

1.2 Subjects and Methods

Thirty five women who had breast tumors detected by X-ray mammogram were subjects for the optical imaging. The age of the women ranged from 30 to 84 years old. Of them, 15 patients had had the lesions removed (lumpectomy operation). 20 patients had a single suspicious small tumor shadow in the mammography. The tumor sizes ranged from 3 mm to 1 cm diameter. The post-operative scar tissue contained seroma. The size of the post-operative lesions were 2 cm to 5 cm in diameter. Approximately thirty percent of the patients had fibrocystic disease.

For the optical measurement, the breasts were compressed gently with two surface holders located parallel to each other (Figure 1). One surface holds an incident lightguide and the other holds a lightguide coupled to a detector, photomultiplier. In between the two lightguides, time resolved spectra of the breast are acquired through transmittance mode. Then, points of the lightguides on the two surfaces are moved 5 mm equally to obtain a two dimensional transmittance image. During the acquisition, lightguide separation is fixed and constant.

Fig. 1. The scheme shows the set up for the optical breast imaging. The breast is gently compressed with two surface holders located parallel to each other. One surface holder contains an incident lightguide and the other holder contains a lightguide coupled to a detector. In between the two lightguides, TRS data of the breast are acquired through transmittance mode.



The time resolved spectrometer (TRS) consists of two wavelength pulsed lasers, which emits light at 780 and 830 nm, a photomultiplier (gallium arsenide), a time amplitude converter (TAC), a photon counting system, and the data stored in a personal computer through an A/D converter. The time width of the pulsed laser light is 300 picoseconds through the TRS system and is used to determine instrument function. This time resolution of the instrument function is good enough for human breast spectra to be used without deconvolution because the tissue spectra gained the half width more than 5 times larger than the instrument function. The two tissue spectra at the two wavelengths are acquired simultaneously by time sharing (delaying one pulse by 10 ns).

The two tissue spectra with wavelengths at 780 nm and 830 nm are analyzed to obtain absorption and scattering coefficients with a curve fitting program, which in principle, is based upon a diffusion equation using semi-infinite boundary conditions (Patterson, et al) (3). Here, scattering coefficients are mainly calculated at maximum photon arrival time. This requires 15 to 20% of early arrival photons. The absorption coefficient is mainly calculated by the decay curve of the spectra, requiring 25 to 50% of the early arrival photons. Hemoglobin saturation with oxygen (SaO₂) is calculated using the two absorption coefficients (4). As a presentation of blood volume, the two absorption coefficients are averaged. Scattering coefficients at two wavelengths are also averaged to yield a scattering image.

Three independent pieces of information are used to process three images from a set of measurements: 1) the oxygen image is based upon hemoglobin saturation with oxygen, 2) blood volume image is from absorptions, and 3) scattering image is from scattering coefficients. Once these three are calculated, they are fed into the image processing program, which translates the location of lightguides on the breast surface as a pixel of the image. It therefore creates images of a 5 mm² resolution. Usually a 5 x 7 pixel image is acquired.

1.3 Results

It is found that the ability to detect breast lesions by the time gated optical method depends upon the size of lesions, the thickness of the breast and contents of breast tissue (fat and fibrous tissue). Usually post-operative lesions can be seen in our optical images, but a small cancer mass of less than 1 cm in diameter is not detectable with 5 to 10 cm thick breasts. Here, we show 3 patients who have post-operative lesions with optical images and a corresponding MRI (Magnetic Resonance Imaging).

Case No. 1

The optical images shown in Figure 2 to 5 are from a 38 year-old patient. Her cancer was removed one month previously (lumpectomy), and under pre- and post-radiation therapy, respectively. Figures 2 and 3 show post-lumpectomy, pre-radiation images. Figures 4 and 5 show post-radiation images.

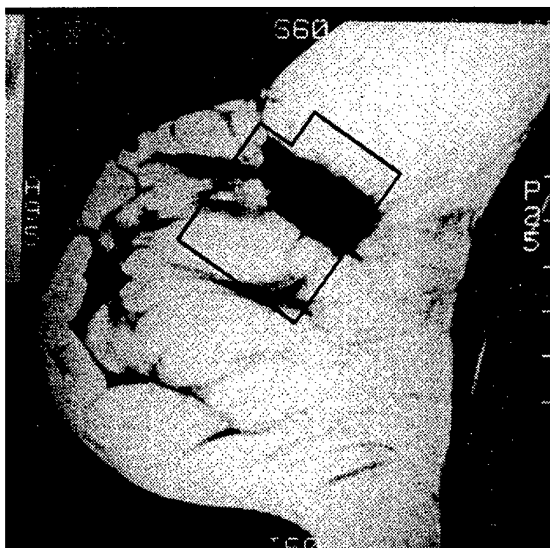


Figure 2. MRI (lateral slice) of case 1, whose cancer was removed (lumpectomy) one month previously. This MRI was taken prior to radiation therapy (pre-radiation). The closed area shows the area where optical imaging was conducted (see Figure 3). Also note that a 2 x 1.5 cm seroma is seen in the location where the lumpectomy had been performed.

The lightguide separation was 6 cm. The seroma had less oxygen concentration; O_2 saturation in Hb is 82% in the seroma and 85-87% in the surrounding tissue pre-radiation (Figure 3-C). After radiation therapy, the size of the cyst became reduced and formed a heterogeneous fibrotic tissue (Figure 4). An overall lower O_2 level was observed in the same area post-radiation as pre-radiation (Figure 5C as compared to Figure 3C), and similar heterogeneity was observed in the area where the smaller seroma is located. The area where the seroma and fibrous scar tissue are located has less blood volume (less absorption (Figures 3-B,5-B)) and more scattering (Figures 3-A, 5-A).

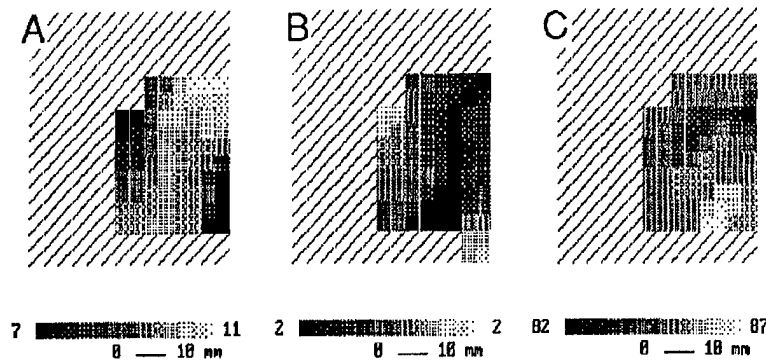


Figure 3. Optical images of case 1, under pre-radiation corresponding to Figure 2. A: scattering image. B: blood volume image C: oxygen image. Note that the seroma has low oxygen concentration than the surrounding tissue.

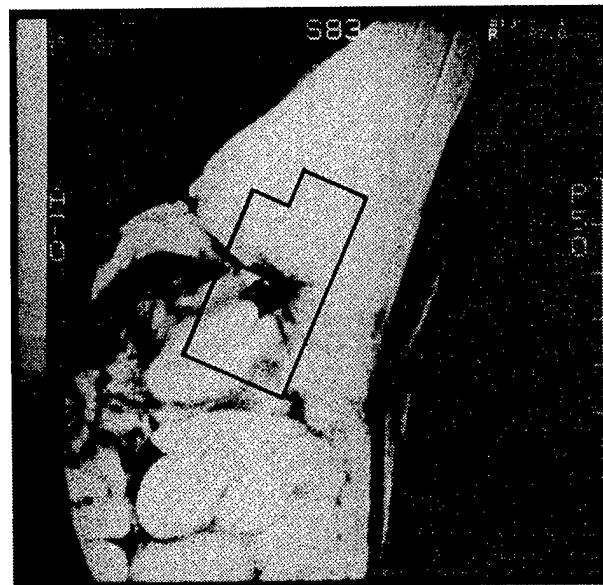


Figure 4. MRI of case 1, after a radiation therapy. The closed area shows the area that optical imaging was conducted (see Figure 5). The size of the seroma became reduced and formed a heterogeneous fibrotic mass after the irradiation.

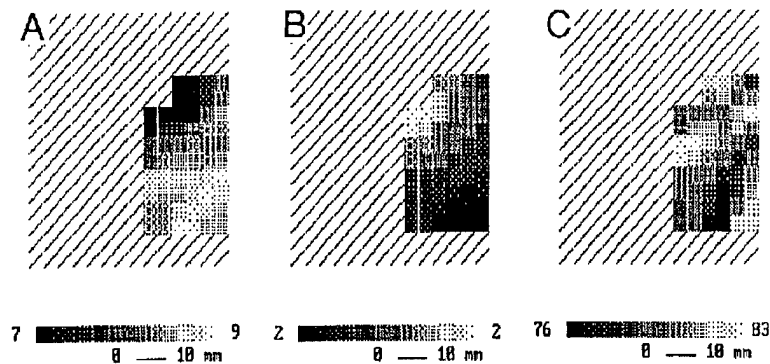


Figure 5. Optical images of case 1, post-radiation therapy, corresponding to Figure 4. A: scattering image. B: blood volume image C: oxygen image. The lesion shows more scattering and contains less oxygen than the surrounding tissue.

Case No.2

The MRI and the optical image (Figures 6,7) are from a post lumpectomised cancer patient. She is 48 years old who has small to medium size breasts. A small lightguide separation of 4 cm was used. After lumpectomy, there is a 4.5 x 2.5 cm mass consisting of fibrotic scar tissue and seroma in the middle of her breast (Figure 6). The optical images were taken laterally covering between seroma and fibrotic tissues. The oxygen image shows that a part of the seroma has a low oxygen level indicating a quite heterogeneous profile (Figure 7-C). The oxygen level in the seroma capsule is particularly higher than the surrounding tissue. The blood volume image shows that the seroma has less blood volume (Figure 7-B). In addition, there is heterogeneity in the scattering images in the seroma as well as in the surrounding fibrotic tissue (Figure 7-A) constructing an image of scar tissue.

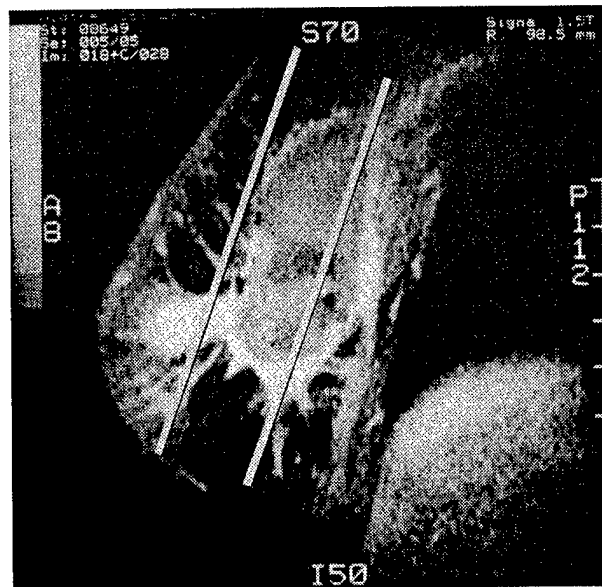


Figure 6. MRI of case 2, who has a large lesion after a lumpectomy. The lesion consists of seroma and fibrous scar tissue.

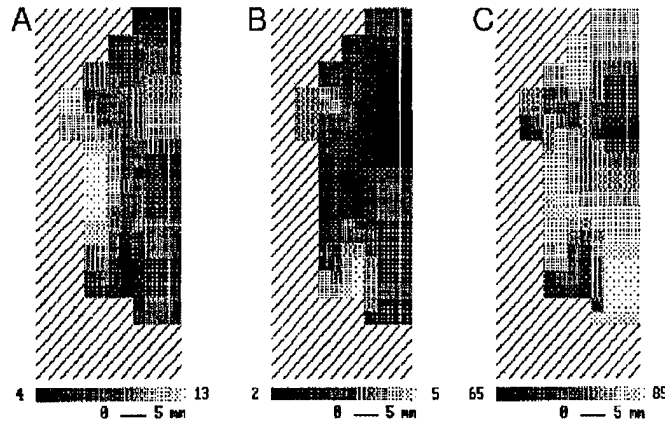


Figure 7. Optical images of case 2. The images were taken in the cranio-caudal direction. The illumination was along the direction of indicated lines and between two lines (Figure 6). The line nearer to the nipple corresponds to the left line of each image. The right side of the images clearly shows the lesion. Note that the lesion has a location with lower oxygen which also scatters more than surrounding tissue, indicating heterogeneity.

Case no.3

The patient is 52 years old and weighs 180 lbs. Her tumor in the breast has been determined to be cancer by biopsy. She already had been treated with a lumpectomy followed by radiation therapy (Figure 8). The optical images (Figure 9) were taken with cranio-caudal direction. In the optical scattering image (Figure 9-A), there are two highly scattering masses, connected to each other by a capsule like structure. This capsule like structure has higher oxygen tension than in the two masses (Figure 9-C). The two masses differ in blood volume (See Figure 9-B), and the one nearer the nipple has more blood volume than the other.

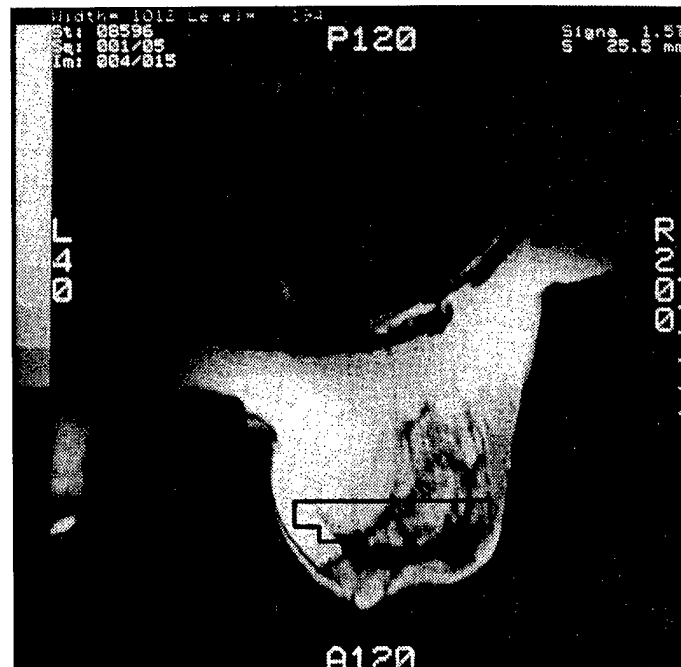


Figure 8. MRI (cranio-caudal direction) of case 3, post-lumpectomy. The closed area shows the area in which optical imaging was conducted (see Figure 9).

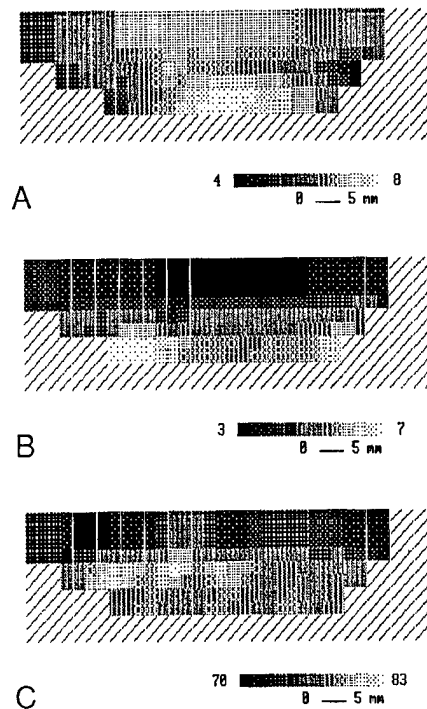


Figure 9. Optical images of case 3, corresponding to Figure 8. A: scattering image. B: blood volume image C: oxygen image. There are two highly scattering masses connected to each other by a capsule like structure. This capsule has higher oxygen tension than in the two masses.

1.4 Discussion

Clearly, we have demonstrated that the time gated optical imaging technique is capable of imaging a relatively large object. However, this technique does not yet clearly detect a small cancer (generally smaller than 1 cm), therefore we did not include those small tumors in this report. It is shown that the time gated imaging system is not yet as precise as X-ray mammography for lesions smaller than 1 cm in size. However, it is certainly better than the current diaphanography in principle.

In the optical imaging technique, the main cause responsible for low resolution of an image is photon diffusion. For the human breast image, conditions for the continuous wave technique (any technology which uses CW light or current diaphanography) are viable in breasts that are small, thin and fatty, and having tumors larger than 1 cm in diameter. Since the CW technique will not satisfy most of the needs for early detection of breast cancers, we have developed a time gated photon imaging system to test feasibility for the purpose. Scattering and absorption images use only 15-20% and 40-50% of early arriving photons, respectively, which therefore eliminates most of the diffusive photons that create obscurity. The results show that the scattering image may have more clear images of lesions than those used for absorption (oxygen and blood volume images) because of narrower time windows for scattering images.

It is clear that this time gated system is not adequate to show a high contrast of lesions of less than 1 cm in size from surrounding tissue. The cause of low resolution comes from many factors. First, although fortunately the breast contains substantial amounts of fat, whose scattering factor is low compared to any other tissue constituents, contrast between fat and fiber versus tumor is not always substantial enough. Secondly, differences of oxygen tensions or blood volumes between those tissue components also may not be substantial enough for the available signal levels. Thirdly,

the technique we use here presents a number in a pixel as a mean value of a long tissue mass across the two lightguides, and can not represent a small lesion.

These problems can be solved by finding causes of obscurities. A more sophisticated image reconstructing technique such as inverse recovery technique (5), will better adapt photon diffusion characteristics into the image construction procedures. In addition, we will be able to obtain higher resolution images with the phased array system and with a contrast agent, such as cardiogreen, which may accumulate in the lesions with permeable capillaries and more circulation. We are in the early stage of developing the optical imaging, and in the future, attempts to improve substantially the quality of optical images will be pursued.

2. TRS STUDY OF OPTICAL CHARACTERIZATION (Years 1 and 2)

2.1 Introduction

We have used the TRS device to image breast tumors with optical outcomes; absorption coefficient and scattering coefficient are shown in Section 1. At the same time, the data can be analyzed quantitatively. The patient population studied consisted of two major populations; tumor bearing breasts and post surgical breasts (lumpectomized). The purpose of separating lumpectomized breast from tumor bearing breast was to seek out some differences in the post operative breasts and tumor bearing ones. It is interesting to see if the X-Ray-dense fibrocystic breast can be recognized by the optical means. In this sense we separated the fibrocystic disease with tumor from simply tumor bearing breasts even though there were only three patients in this category. In the total of 63 patients studied, we are able to analyze 51 patients' data at this point.

2.2 Methods (TRS)

For the optical measurements using TRS, the methods are described in detail in Section 1. The data were taken usually at a selective area of the lesion, 2 to 4 cm square area of the planes created by mildly compressing side by side or up to down direction. The patients usually had between 25 to 64 points of measurements dependent upon the area of lesions. The optical data analysis are available with fully developed software. In brief, the time resolved spectrum is fitted in diffusion equation (6) with the minimum square root method. The data are averaged to present only with one value from one subject.

2.3 Results (TRS)

The breasts of 51 subjects were analyzed quantitatively at this point. The patient populations were divided into three categories; lumpectomized, tumor bearing, and fibrocystic breasts. Table I shows the mean and standard deviation of the μ_a , μ_s and oxygen saturation with hemoglobin in the normal, lumpectomized, tumor bearing, and fibrocystic breasts. The absorption coefficients in the normal population (n=18) have a lowest mean values (0.025), and all three patient populations have double the value of μ_a (see Figs. 10 and 12). The scattering coefficients follow similar high values to μ_a . In the fibrocystic breast, μ_s was much greater than any other group, i.e., three time higher than the normal breasts in the three subjects we measured (see Figs. 11 and 13).

Table I. Optical Characteristics in the Patient Populations

	Normal	Lumpectomized	Cancer	Benign Tumor	Fibrocystic Disease
N	18	23	7	13	8
μ_a	0.025 0.008	0.059 0.028	0.046 0.031	0.055 0.041	0.059 0.044
μ_s	11.0 3.0	14.9 6.6	14.8 2.8	14.5 4.7	17.4 5.5
SaO ₂ %	60.2 17.5	59.1 8.4	56.8 9.7	61.6 9.7	55.2 6.1

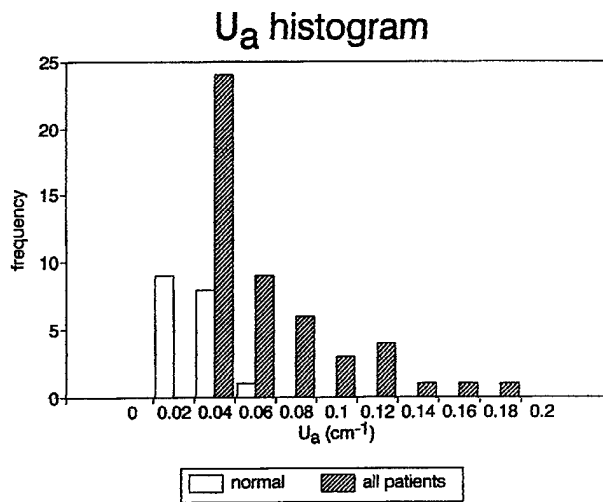


Fig. 10. Histogram of the absorption coefficient with all patient populations and normal controls.

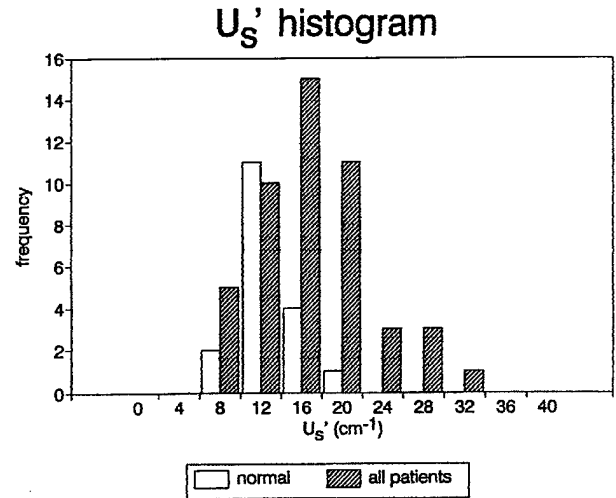


Fig. 11. Histogram of scattering with all patient populations and normal controls.

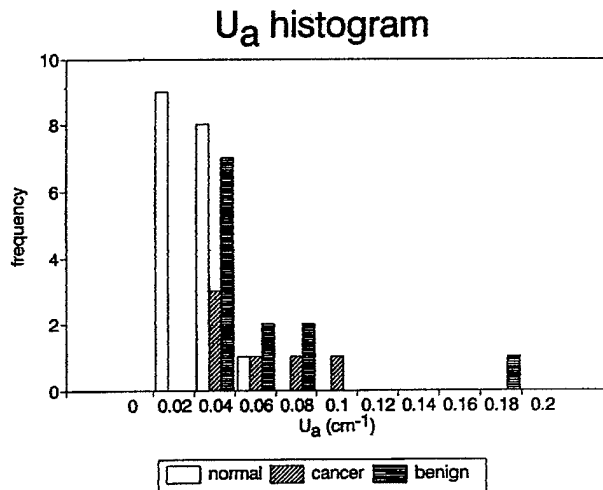


Fig. 12. Histogram of μ_a : absorption coefficient with patients: tumor bearing and normal control. A greater absorption coefficient is seen in the patient population.

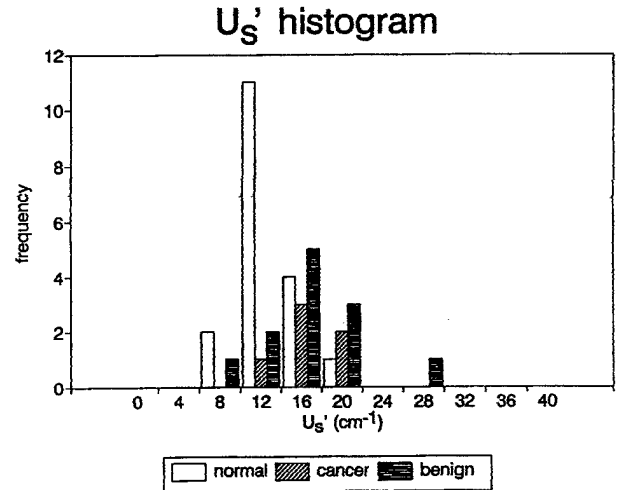


Fig. 13. Histogram of μ_s' in the patient populations: tumor bearing breast, and normal controls.

The above μ_a histogram is a display of the tumor bearing breast (cancer and benign tumor) as compared to normal controls. A greater μ_a is seen in the tumor bearing populations. The histogram of μ_s' is of the tumor-bearing breasts (cancer and benign) as compared to normal control subjects.

2.4 Discussion

We expected that because tumor growth is usually accompanied by angiogenesis and higher blood flow, high blood content could be seen and it seems that is the case presented in this study. Also, lumpectomized breasts within 2 weeks should still produce higher metabolism because of the

healing process, leading to such high absorption coefficients due to high blood contents. It will be interesting to see the effect of time after surgery on μ_a .

It would be very interesting if we can analyze more precisely those μ_a and μ_s' values related to the specific lesion. However, we do not know the exact location of the lesion at the time of the optical measurement which prevents the tumor from being analyzed with regard to μ_a and μ_s' more closely. Therefore, only one way to analyze the tumor characterization is during another measurement such as MRI and X-Ray mammography. That is exactly what we did in the trial for the last phase of this study. It is not surprising to see the hyperemia near the tumor tissue, within the 2.5 array. Also, it may be true that in a small tumor, this hyperemic area may be much larger than the area of tumor itself.

Further analysis of the rest of unanalyzed patients and controls may provide statistically significant results for μ_a and μ_s' . The increase in μ_a can indicate some unusual breast metabolic activity, which can be used for screening purposes.

3. PRESENT AND FUTURE PLANS FOR THE TRS SYSTEM FOR OPTICAL CHARACTERIZATION IN TUMOR BEARING BREASTS

The detailed tasks undertaken in 1995-6 are in accord with the 1994 proposal: the development of technology for in-magnet recording of photon migration data on human breast is considered mandatory for the following reasons:

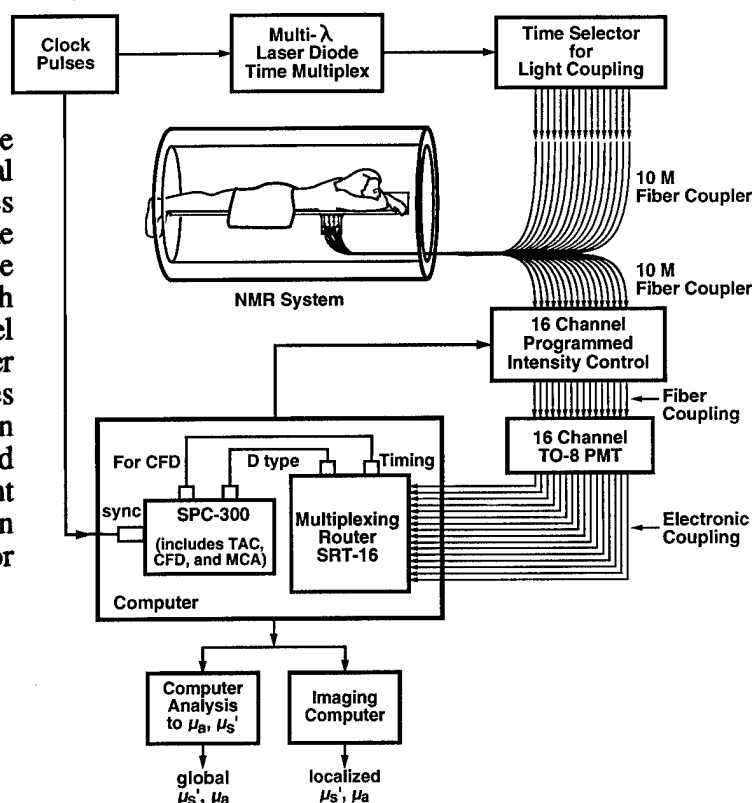
1. Co-registration of MRI and TRS imaging is immediately possible.
2. Access to the patient population and to facilitated patient consent is assured.
3. *A priori* knowledge of the location of the tumor from MRI (and X-ray mammographic) coordinates facilitates the imaging of the tumor and the calculation of its scattering (μ_s') and absorption (μ_a) properties.
4. Advanced algorithms have now been developed for creation of images of tumors from several millimeters to better than 1 cm in resolution and as mentioned above for calculating the tumor's optical properties. Such algorithms are described in the Ph.D. Theses of Dr. David Boas (6) and Dr. Maureen O'Leary (7) and in a recent contribution by Xingde Li (8). All these algorithms can effectively be applied to the experimental data gathered in the NMR magnet.
5. Sensitivities available to the optical method: The availability of μ_a and μ_s' data for the tumor volume and for the adjacent area enables the calculation of:
 - a. Increased blood concentration in a tumor due to hypervascularization.
 - b. Decreased oxygen saturation in the tumor due to hypermetabolic state of the tumor with respect to the surrounding breast tissue.
 - c. Intensity response to cardiogreen (due to indocyanine green, ICG). This is a vascular probe which not only indicates immediately the vascular volume, but over time, indicates the extent and course of its extravasation, generally used now with MRI to indicate malignancy.

Light scattering and absorption of tumor bearing human breast has been studied in a large number of X-ray mammographically studied patients. Time domain data acquired using the methodology of Fig. 14 enabled a frequency domain analysis to be made by Fourier transformation.

3.1 Experimental Methods/Results Obtained

Transformation from Time to Frequency Domain. In the foregoing tasks we have proposed both time domain and frequency domain methods to be studied and to be evaluated for the efficacy in breast tumor detection (9). Furthermore, these methods have required significant development in the course of the research and finalization of the designs of both these methods has been achieved. Preliminary data has been obtained on model systems which can afford the basis for extending the studies to an appropriate size of tumor bearing population as had been contemplated in Table I of the original application and where in the year 1 report, the three methods were described ((See Appendix I for Table) and a series of patients expected to be studied. In order to satisfy the needs of this table, over 1,500 studies were made. A special report was made of 23 observations on the oxygen saturation in the tumor bearing breast (see below). Furthermore, histogram displays of μ_a and μ_s' for human breasts with small tumors were made to establish the distribution of values to be expected using the "banana" pattern optical detection of tumors.

Fig. 14. A detailed diagram of the components for in-magnet TRS Optical Tomography system. The clock pulses trigger the laser and the TAC. The time selector affords variable timing of the selection of fibers for general search and for localized quantitation. Parallel detection of the optical signals together with parallel processing achieves optimal signal to noise ratio. Photon outputs through the breast are adjusted in intensity for each position of the light source to ensure optimal photon counting conditions. Computers for image reconstruction are provided.



Year 2 reported detailed studies of a total of three groups of patients, which gives a total of 140 examinations validating the required studies of Table 1 (Appendix I). 23 subjects were examined for oxygen saturation which showed that 50% of the breasts to be in a hypoxic state, and therefore, potentially radiation resistant.

Future plans for Year 2 involved the setting up simultaneous gadolinium enhanced MRI and cardiogreen enhanced optical tomography in order to obtain greater specificity/sensitivity, and indeed, co-registration of the images. This has necessitated substantial instrumentation development according to Fig. 2 of the Year 2 Report (Appendix II) for which additional funds were recruited

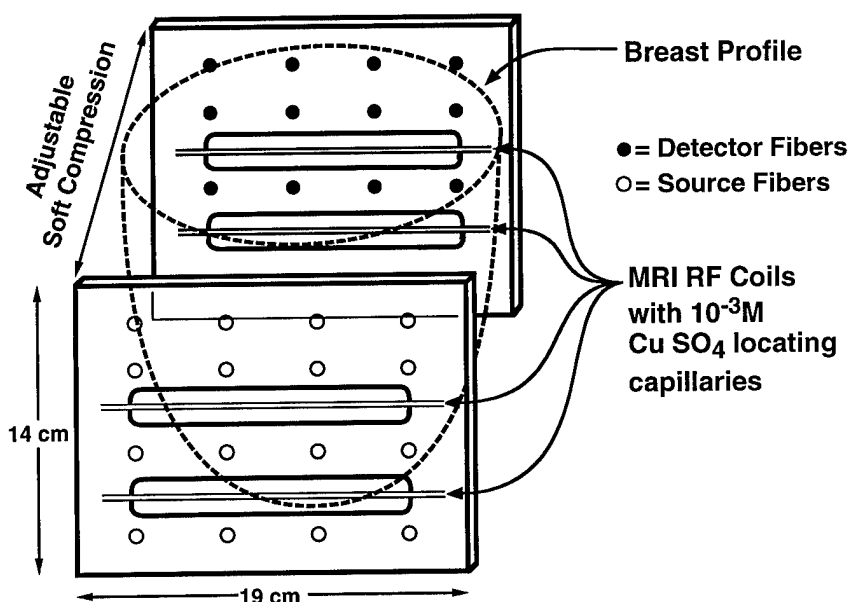
(Fig. 14 above). Furthermore, a phase modulation system was developed in order that 1 to 1 comparison of the two systems might be available for further work under Army Contract support.

3.2 Co-Registration System: MRI/Optical Imaging

The preliminary diagram of this system presented in Fig. 2 of the Year 2 (Appendix II) report is now evolved as in Fig. 14 above. The system consists of a 16-channel source detector system with a multiwavelength laser diode illumination. This illumination is time sequenced through 16 fibers to successively illuminate the breast in 16 positions at multiple wavelengths, usually 760 and 780 nm and, in some cases, 830 nm. The laser diode power is within the FDA limits of approximately 20 microwatts and is delivered in pulses of 20 to 100 pico second duration. 16 detectors simultaneously observe the photon migration signals by transmission through the breast and measure the photon kinetics at the various positions at which available signal to noise ratio is obtainable. The 16 channels are selectively processed by a multiplexer router (Edinburgh Electronics or EEG Electronics) and thus multichannel analysis is available at the time course at the selected wavelengths and at the selected positions. The data on photon migration is stored in a computer which may be analyzed according to the algorithms used previously in the year 2 survey, or by imaging algorithms which have been developed by Boas and O'Leary (6,7) and are discussed as a part of this final report.

The implementation of this device in the 1.5 T magnet is illustrated in Fig. 15 which shows the orientation of the 16 source/detector combinations with respect to the NMR coils. Furthermore, small capillaries are filled with water and 1 millimolar copper sulfate in order to mark clearly the relationship between the NMR coils and the optical fibers.

Fig. 15. Optical coupling to the soft compression plates for MRI imaging as shown by the open circles for sources and the solid circles for detectors. The fibers will lie parallel to the plates because of the right angled prisms.



3.3 Current State

This apparatus has been assembled using 8 channels and a microchannel plate detector. 16 PMT's (photomultiplier tubes T08) have been ordered from Hamamatsu and will be delivered shortly. This is more efficient than the microchannel plate and has less crosstalk.

4. CWS BREAST IMAGING WITH CONTRAST AGENT (Years 2 and 3)

4.1 CWS Methods

Eight or 16 combinations of light sources (tungsten bulbs) and light detectors (silicon photodiodes) are located on a two dimensional circle line equal distance apart from each other (22.5° or 45° angle apart, Figures 16A,B).

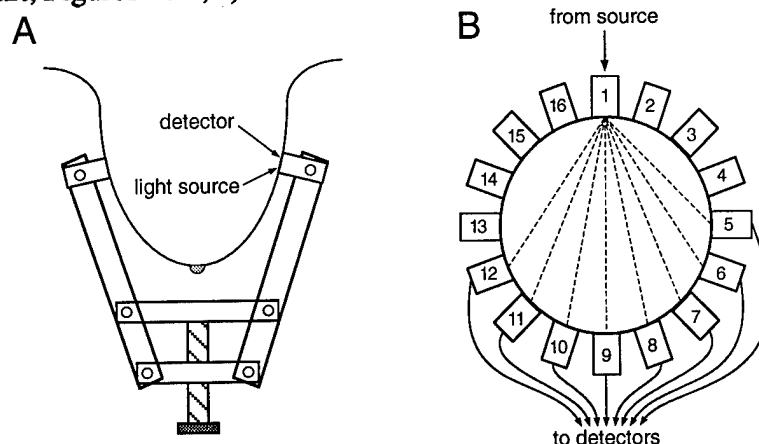


Figure 16. The scheme A describes the cut section of the 16 light source-detector device, holding a human breast inside. The diameter can be fitted easily with set screws. When the device fits a breast, source detector relation remains unchanged (B).

4.2 Image Algorithm, Back Projection

The original back projection algorithm has been developed for the CAT scanned data. Since that application deals with straight rays, when it is applied to diffusive rays of photons, modifications must be made to adapt the characteristics of the photons. Firstly, the idea of "photon hitting density" (5) replaced the linear relationship of X-ray when the locations of beams are translated into pixels. Photon hitting density is the probability of a photon occupying a specific place in between a source and a detector. Figure 17 shows the area where photons can be localized with approximately 80 to 60 % probabilities when it is assumed that μ_a and μ_s' are known to be similar to the human breast and homogeneous.

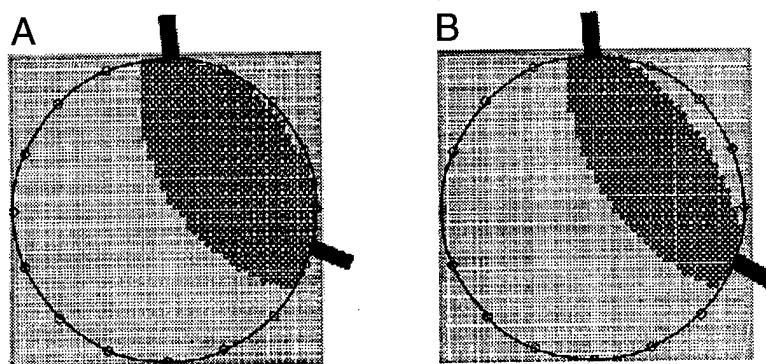


Figure 17. Photon hitting density image of breast. Approximately 80(A) to 60(B) % of the photons will pass through these shaded area.

In the image re-construction program, the probability is translated into a weight factor when it is used to process back projection. The back-projection is basically a process averaging out values of

information that each beam carries with the weighing in each pixel. Therefore we can not recover correct values, which is attenuated or amplified by the surroundings.

4.3 CWS Model Study

In the circle, we placed a breast model using 0.5% intralipid and ink (about the same scattering and absorption coefficients as those in the breast tissue). It takes only a few seconds to acquire data since one source is on. All the detectors detect the photons at the same time. 16 sources cycle at a rate of 200 msec/source (Fig. 18).

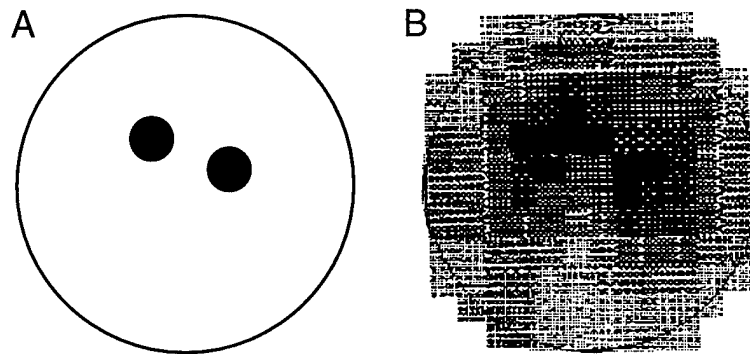


Figure 18. The model study of optical imaging with the 8 probes. Intralipid 0.5% and ink resembles the optical characteristics of the human breasts. Two 1 cm objects are located 1 cm apart. When 8x8 images are made, the two objects are depicted in the reconstructed image by the back projection algorithm.

The data acquisition for an image takes 4 - 8 seconds with 8x8 or 16x16 data points. A contrast agent; Indocyanine Green (ICG, 0.25 - 0.5 mg/kg), is injected in the model system similar to treating human, when data are being acquired continuously every few seconds over 10 - 15 min as the ICG absorption signal appears and disappears. Data are processed as OD changes due to ICG from the iv injection. Some data points are averaged in several time windows and as a result, several images are reconstructed using back-projection algorithm. The results show that with the ICG concentration which we inject into humans, apparent resolution is 7 mm for the contrast agent.

4.4 Human CWS Imaging with Contrast Agent

The patient (56 years old) has a long history of a palpable tumor. The lump swells with menstruation cycle. When ICG is injected, optical image depicts the lesion area (Fig. 19, MRI), and contrast of the lesion are great at the following minutes (2 - 4 minutes, Figs. 20C-6E) in the 16x16 image. It reveals that a functional tumor like this also has a greater circulation and is associated with a high accumulation of ICG. The contrast agent makes it possible to depict the tumor in this case.

In the same patient, MRI shows a colony of small fibrous cysts, with ducts which are hypertrophic and connected to the nipple (see Fig. 20 MRI).

The results show that the resolution of tumor detection is enhanced a great deal (note the comparison between Figs. 19A and 19C). It also shows that some of the benign tumor will be detected and further diagnosis has to be made after this type of image. It is possible that we could find a way to distinguish a malignant tumor by the optical characteristics, such as by a combination of μ_a and μ_s' in malignant tumor, or contrast agent time course kinetics due to leakage of vessels with high angiogenesis activity etc. These are still yet to be studied.

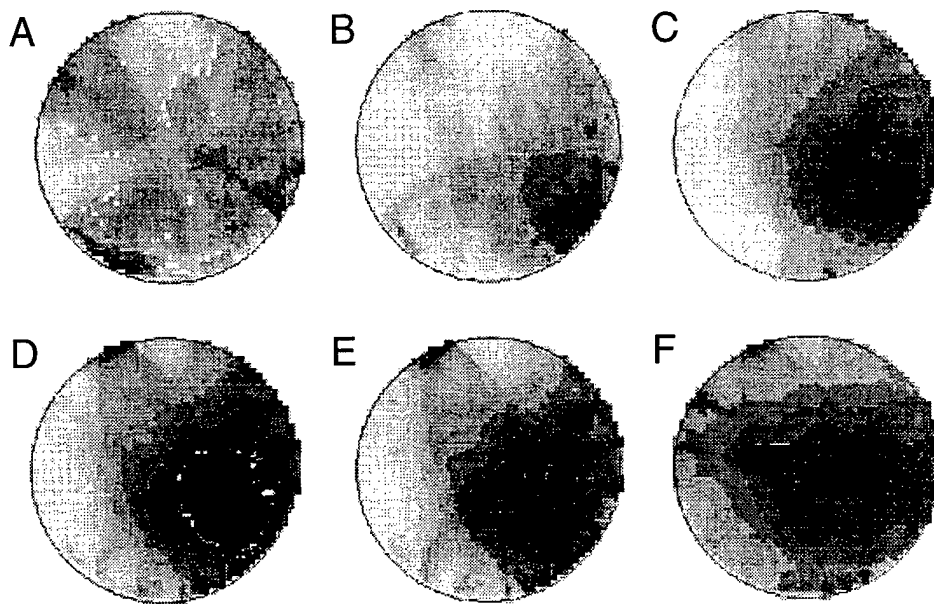


Figure 19. Optical images of a breast with fibrocystic disease with ICG injection at B.
A – pre-injection. B-F correspond to one minute images after the ICG injection (1-5 min).

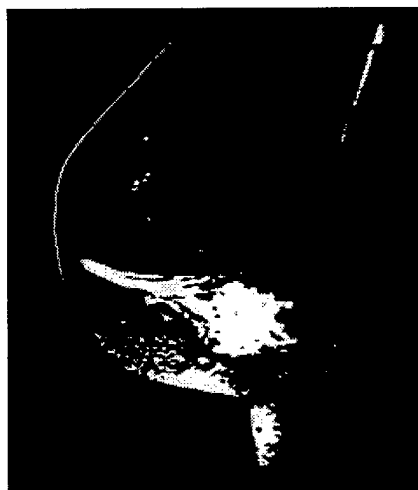


Figure 20. MRI of a breast with fibrocystic disease. Gadolinium accumulation is seen in the swelling ducts of the cyst.

5 IMAGING USING THE FREQUENCY DOMAIN METHOD (Years 2 and 3)

5.1 Phased Array Imaging

The rapidly modulated light obtained from a laser diode can be employed equally well and affords a somewhat more compact system for breast tumor detection. In this case, the breast is immersed in matching intralipid as shown in Fig. 21 and a dual wavelength scanner is electro-mechanically passed by the breast immersed in the above mentioned matching fluid. The tank is wide enough to accommodate the larger than average breast.

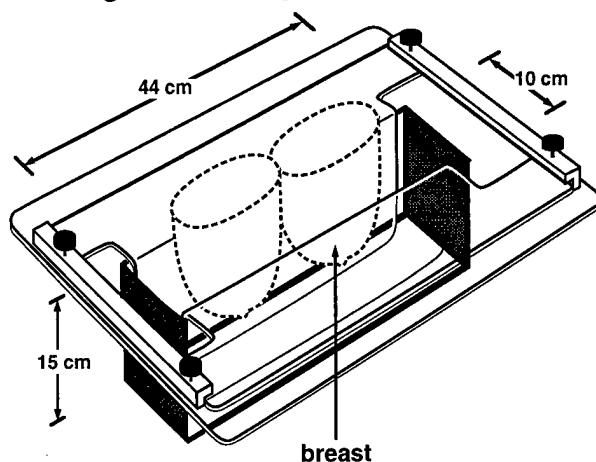


Fig. 21. Illustrating a breast scanner with pendent breast (in Saran wrap) immersed in matching intralipid, ink $\mu_a = 0.02$, $\mu_s' = 10 \text{ cm}^{-1}$ (warmed to body temperature, sources and detector translated along box at appropriate heights).

The performance of this device is indicated in scanning of model breast which is occupied by the equivalent of a half milligram per kilo cardiogreen (ICG) compound. The ICG is the choice of agent for use in our studies as a complement to the galdolium chelate, and is also useful for the MRI. In this case, the trace shows the detection of the location of a 1 cm diameter tube containing 6 micromolar ICG so that the active volume seen by the probe is approximately 12 nanomoles of the cardiogreen, an amount that can be expected to be obtained in a 1 gram tumor (see Fig. 22).

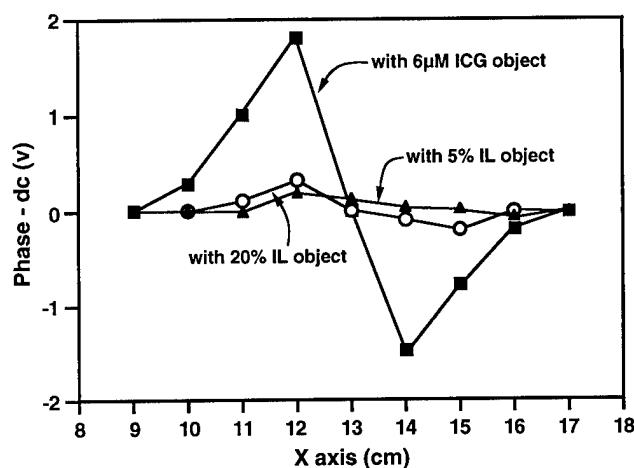


Fig. 22. Illustrating the accuracy of location of a 1 cm^3 object filled with $6 \mu\text{M}$ ICG. The object is located at the zero volts intersection $\pm 1 \text{ mm}$.

A PMS system (50 MHz, NIM Inc.) with 5 mwatt 780 nm laser diodes, having two phase 0° and 180° angle was used for imaging. These two lasers are located on the circular surface at 22° or 45° angle, while the detecting lights from 360° angles with lightguides 16 or 8 respectively, similar to the CWS imager (Figure 23). A tumor model with intralipid 0.5% and black plastic rod cylinder was placed in the intralipid container.

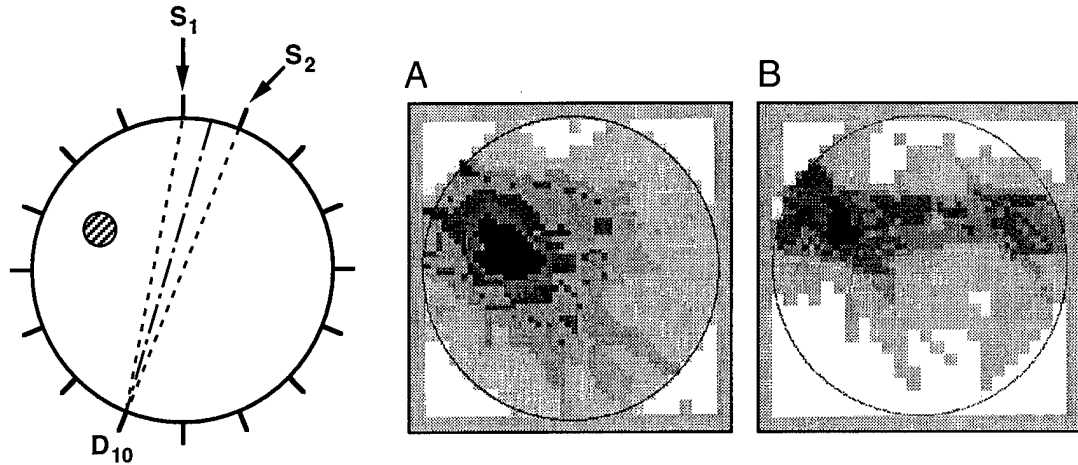


Figure 23. PMS image of single object model (black plastic rod 0.8 cm) with 0.5% intralipid surrounding in a 8 cm container. (Left) Schema for 8 probe imager. Two sources (S_1 , S_2) are located at 45° from each other. Detector 6 receives phase shift from the two light sources. A. image using 8 x 8 imager. B. image using 16 x 16 imager.

5.2 Imaging Developments: FFT Approach to Biomedical Imaging with Diffusive Photon Density Waves.

In recent years, a variety of techniques for imaging turbid media such as tissue with diffuse light have been explored. Most of these methods employ direct matrix inversion (e.g., singular value decomposition) or iterative techniques (e.g., ART, SIRT and Conjugate Gradient) for image reconstruction, and they are in general computationally intensive. In this paper, we introduce a new imaging methodology which is computationally much faster. Our approach is essentially a near-field wave technique that relies on a series of 2-dimensional fast Fourier transforms (FFT's). We present a rigorous account of the theory, and the first experimental images of absorbing and scattering objects in turbid media using the approach. In addition to producing information about the position and shape of the hidden object(s), we have found that under some circumstances it is possible to utilize projection images to deduce the optical properties within a thin slice without the need for a complex reconstruction procedure such as matrix inversion. It should be possible to obtain clinical projection images in real time with this fast FFT approach. (10)"

This method (See Appendix III) has recently been used to obtain images of two normal adult human breasts, in one case with the tumor phantom in the breast chamber of Fig. 21, as presented at the SPIE 1997 meeting.

In this study the cancer was not seen in the X-ray mammography, but was palpable (pea size). The image was reconstructed primarily by a near-field wave technique that relies upon a series of 2-dimensional FFT's as described above.

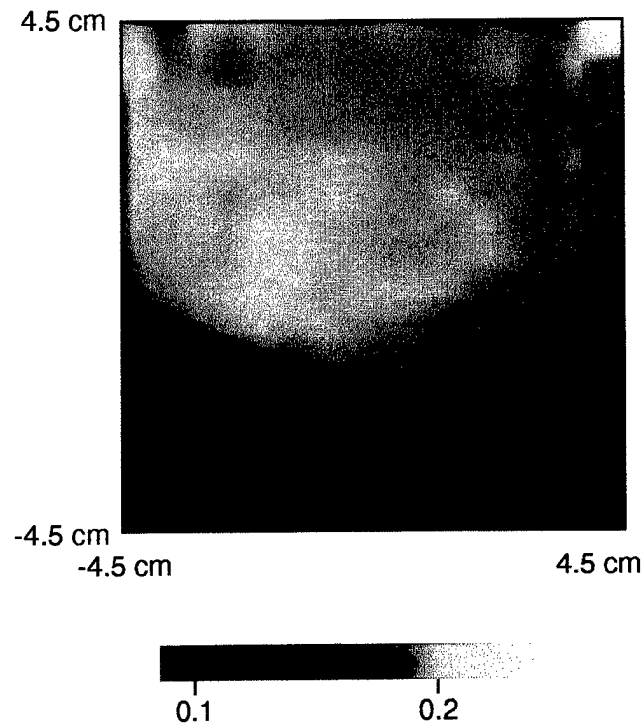


Figure 24. The breast image presents μ_a (calculated from the frequency domain system) on a patient with a cancer close to her chest (upper right)

CONCLUSION

We demonstrate here that with three different technologies, we can detect cancers. It is however premature to conclude resolution limitations of each technique at this point. The resolution we presented here in TRS images is in a range of 1 cm, but this photographic image is not a valid way to judge resolution, because the thickness of the breast has not been resolved in the current method. However, this study has shown that it should be much better than 1 cm resolution when the thickness of the breast can be resolved. Surprisingly, the diffusive CWS has a potential for imaging human breast lesions. The key for the success is to produce higher contrasts by the use of contrast agents with the modified back-projection algorithm. However, we show here an example of the benign tumor, which clearly indicates greater blood flow and blood volume in the hyperactive benign tumor. A serious question here is does the blood flow- blood/volume image really diagnose a malignant tumor? We can only answer this question by studying more cancer cases as well as benign tumors and compare these two.

The next step is to search for the specificity of a malignant tumor. We now know that to image the high circulation, blood volume does not necessarily identify the malignancy because it shows a hyperactive metabolism or the heterogeneity of the tissue metabolism. The other function of high circulation high blood volume image has to be considered. For example, an unusually high permeability constant or diffusion coefficient of ICG into the lesion may identify malignancy. The contrast method we used may help identify malignancy by observing the time-distribution relationship of the contrast agent.

Many previous investigation have indicated that oxygen concentration in cancer is much lower than in the normal tissues (11). Benign tumors do not have such low oxygen concentration (11). The oxygen image should be considered as a potential diagnostic image for cancer. Oxygen images can be easily obtained by adding the information of multiple wavelength data.

REFERENCES

1. Kang, K.A., Chance, B., Zhao, S., Srinivasan, S., Patterson, E. and Trouping, R. (1993) Breast Tumor Characterization using Near-Infra-Red Spectroscopy. SPIE Proceedings Vol. 1888 Photon Migration and Imaging in Random Media and Tissues (Chance, B. and Alfano, R.R., eds.) SPIE, Bellingham, WA, pp. 487-499.
2. Chance B, Leigh JS, Miyake H, et al. Comparison of time resolved and unresolved measurements of deoxy hemoglobin in the brain. Proc. Nat. Acad. Sci. 85:4971-4975. 1988.
3. Patterson MS, Chance B, and Wilson B. Time resolved reflectance and transmittance for the noninvasive measurement of tissue optical properties. J. Appl. Optics. 28:2331-2336. 1989.
4. Sevick EM, Chance B, Leigh J, Nioka S, Maris M. Quantitation of time- and frequency-resolved optical spectra for the determination of tissue oxygenation. Anal.Biochem.195:330-351. 1991
5. Schotland J, Haselgrove J, and Leigh JS. Photon hitting density. Applied Optics. 32:448-453. 1993.
6. Boas, David (1996) Diffuse Photon Probes of Structural and Dynamical Properties of Turbid Media: Theory and Biomedical Applications. Ph.D. Thesis, University of Pennsylvania, Philadelphia, PA
7. O'Leary, Maureen A. (1996) Imaging with Diffuse Photon Density Waves. Ph.D. Thesis, University of Pennsylvania, Philadelphia, PA
8. Li, X., Dunduran, T., Chance, B. Yodh, A.G. and Pattanayak, D.N. (1996) Diffraction Tomography for Biomedical Imaging with Diffuse Photon Density Saves. Optics Letters. in press.
9. Patterson, M.S., Moulton J.D., Wilson, B.C., and Chance, B. Proc. SPIE-Int. Soc. Opt.Eng. Applications of Time-Resolved Light Scattering Measurements to Photodynamic Therapy Dosimetry. In: Photodynamic Therapy: Mechanisms II. Proc. Soc. Photo Optical Instrum. Engr. 1203:62-75.
10. Li , X.D., Chance, B and Yodh, A.G. (1997) FFT Approach to Biomedical Imaging with Diffusive Photon Density Waves. SPIE (San Jose, February 8-12, 1997) Paper 2979-34, Session 4, in press.
11. Vaupel, P., Kelleher, DK and Gunderoth, M. (eds) Tumor Oxygenation. Stuttgart, New York Fisher 1995.

Bibliography of Publications

Supported by Department of Defense Grant USAMRD, DAMD17-93-C-3071

- Nioka, S., Miwa, M., Ore, S., Schnall, M., Haida, M., Zhao, S. and Chance, B. (1994) Optical Imaging of Human Breast Cancer. *Adv. in Exp. Med. & Biol. Oxygen Transport to Tissue XVI* (M.C. Hogan, et al., eds.) 361:171-179.
- Nioka, S., Yung, Y., Schnall, M., Zhao, S., Orel, S., Xie, C., Chance, B. and Solin, L. (1996) Optical Imaging of Breast Tumor by Means of Continuous Waves. in *Oxygen Transport to Tissue XVIII* (E.M. Nemoto, ed.) Plenum Publ. Corp. in press.
- Chance, B. (1995) Time Resolved Spectroscopy and Imaging. *Proc. of Optical Tomography, Photon Migration, and Spectroscopy of Tissue and Model Media: Theory, Human Studies, and Instrumentation* (Britton Chance and Robert R. Alfano, eds.) SPIE, Bellingham, WA 2389:122-139.

Related Studies Performed under Other Support

- O'Leary, M.A., Boas, D.A., Chance, B. and Yodh, A.G., (1995) Experimental Images of Heterogeneous Turbid Media by Frequency-Domain Diffusing Photon Tomography" *Optics Lett.* 20:426-428.
- Liu, H., Boas, D.A., Zhang, Y., Yodh, A.G. and Chance, B. (1995) A Simplified Approach to Characterize Optical Properties and Blood Oxygenation in Tissue Using Continuous Near Infrared Light. *Proc. of Optical Tomography, Photon Migration, and Spectroscopy of Tissue and Model Media: Theory, Human Studies, and Instrumentation* (Britton Chance and Robert R. Alfano, eds.) SPIE, Bellingham, WA 2389:496-502.
- Boas, D.A., Liu, H., O'Leary, M.A., Chance, B. and Yodh, A.G. (1995) Photon Migration within the P3 Approximation. *Proc. of Optical Tomography, Photon Migration, and Spectroscopy of Tissue and Model Media: Theory, Human Studies, and Instrumentation* (Britton Chance and Robert R. Alfano, eds.) SPIE, Bellingham, WA 2389:240-247.
- Miwa, M., Ueda, Y. and B. Chance, B. (1995) Development of Time-Resolved Spectroscopy System for Quantitative Noninvasive Tissue Measurement.. *Proc. of Optical Tomography, Photon Migration, and Spectroscopy of Tissue and Model Media: Theory, Human Studies, and Instrumentation* (Britton Chance and Robert R. Alfano, eds.) SPIE, Bellingham, WA 2389:142-149.
- Beauvoit, B., Evans, S.M., Jenkins, T., Miller, E. and Chance, B. (1995) Correlation between the Light Scattering and the Mitochondrial Content of Normal Tissues and Transplantable Rodent Tumors. *Anal. Biochem.* 226:167-174.
- Zhao, S., O'Leary, M.A., Nioka, S. and Chance, B. (1995) Breast Tumor Detection using Continuous Wave Light Source. *Proc. of Optical Tomography, Photon Migration, and Spectroscopy of Tissue and Model Media: Theory, Human Studies, and Instrumentation* (Britton Chance and Robert R. Alfano, eds.) SPIE, Bellingham, WA 2389:809-817.

Personnel Supported by Contract DAMD17-93-C-3071

Solin, L.
Chance, B.
Orel, S.
Nioka, S.
Liu, H.
Liu, S.
Zhao, S.
Yi, N.

Appendix I

Table from Original Application and Year 1 Report

PLANNED SCHEDULE OF STUDIES

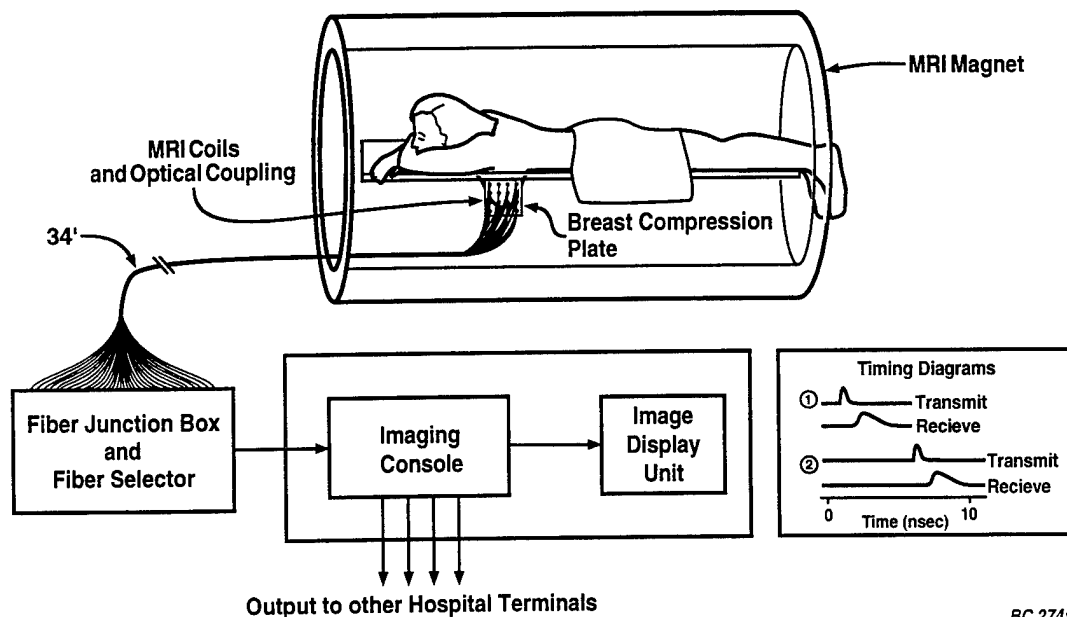
Year	1	2	3
Method 3 (Pulse Time)	+	-	-
Method 3 (Phase Modulation)	-	+	+
Method 4* (Amplitude Modulation)	-	+	+
No. of Studies	120	120	120
Expected Malignant	30	30	30

*120 patient studies with this method are proposed. It is proposed that 50 of these be studied in Years 2 and 3.

Appendix II - From Year 2 report

Future Plans: Aims 2,3, and 4.

As is consistent with Aims 2, 3 and 4, we are proposing as a part of the Year 3 effort and as a main feature of any possible further funding to carry out the optical and MRI examinations simultaneously rather than consecutively since only a small fraction of the available population is willing remain to continue the study with the optical method. The diagram of Figure 2 illustrates our proposal to accomplish this by fiber optical coupling of the optical method directly into the magnet bore through 34 feet of 32 fibers, 16 on each side of the breast, and an additional 16 fibers on the contralateral breast as soon as the MRI has completed the "dual breast" coil assembly, leading to a potential for 64 optical fibers for coupling in and out of the MRI. Enthusiastic support of this project is evinced by the MRI team, particularly Dr. Schnall who has indicated that the soft compression plates used with the MRI are optically transparent and could readily be used to support at least 16 source detector fibers on each side of a single breast, or in fact, both breasts, because MRI plans to observe both breasts simultaneously in order to ensure that no tumors are located in the contralateral breast. Thus, sufficient fibers will be coupled directly into the MRI soft compression plates to afford tumor detection over the entire volume imaged by MRI, and thus ensure correlation of the results of the two methods. Furthermore, the two methods are non-interfering, and optical data can be acquired simultaneously with MRI data since no detectable magnetic field is induced by propagation of light through the optic fibers.



BC 274a

Figure 2. Illustrating a method of procedure for fiber optic coupling of the time domain and phase modulation optical method to the plastic breast compression plate used in the MRI studies. The diagram indicates the use of different fibers in the fiber optic coupling to obtain data from different places on the breast.

Diffraction Tomography for Biomedical Imaging with Diffuse Photon Density Waves

X. D. Li^{†*}, T. Durduran[†], B. Chance^{*} and A. G. Yodh[†]

[†]*Department of Physics and Astronomy, *Department of Biochemistry and Biophysics*
University of Pennsylvania, Philadelphia, PA 19104

D. N. Pattanayak[†]

GE Corporate Research and Development, Schenectady, NY 12301

(Submitted on Nov 11, 1996)

Abstract

The spatial structure of optically heterogeneous turbid media is probed with diffusive light. Projection images are obtained experimentally by deconvoluting the scattered diffuse photon density waves on a planar boundary using a Fast Fourier Transform (FFT). The method is very fast, permitting object localization and characterization in ~ 1000 volume element samples on sub-second computational time scales. The optical properties of slice shape inhomogeneities are accurately determined.

In recent years the application of near-infrared (NIR) diffusing light for biomedical diagnosis and imaging has gained favor as a result of its non-invasive nature, economy, and novel contrast relative to other diagnostics [1-3]. To this end a variety of techniques for imaging with diffuse light have been explored [4,5]. Most of these methods employ direct matrix inversion (e.g., singular value decomposition) or iterative techniques (e.g., ART/SIRT [6] and Conjugate Gradient Descent) for image reconstruction.

In this paper we introduce a new near-field, diffusive wave imaging methodology using techniques similar to those of conventional diffraction tomography [7]. While the near field diffraction tomography method has attracted the attention of a few researchers in the pho-

ton migration field [8], our paper presents a rigorous account of the theory, and provides the first experimental images of absorbing and scattering objects in turbid media using the approach. It differs from least-square techniques such as ART and SIRT in that it is fast and non-iterative. In addition to providing information about the position and shape of hidden object(s), the projection images can be used to deduce the optical properties of heterogeneities without the need for complex reconstruction procedures such as matrix inversion, when the heterogeneities are thin and information about their depth is available.

We adopt the frequency domain picture for our discussion. An intensity sinusoidally modulated light source coupled into a highly scattering medium such as tissue, produces a diffuse photon density wave (DPDW) that propagates outwards from the source [9]. The amplitude and phase of this DPDW depends on the absorption and scattering coefficients within the turbid medium.

In uniform turbid media, the DPDW from a point source at \mathbf{r}_s detected at position \mathbf{r}_d has the form $U_0(\mathbf{r}_d, \mathbf{r}_s, \omega) = M_0 \exp(i k_0 |\mathbf{r} - \mathbf{r}_s|) / (4\pi D_0 |\mathbf{r} - \mathbf{r}_s|)$. Here ω is the angular source modulation frequency, M_0 is the ac amplitude of the source, $D_0 = v / (3\mu'_{so})$ is the diffusion coefficient (v is the speed of light in the medium), $k_0 = \sqrt{(-\mu_{ao}v + i\omega) / D_0}$ is the DPDW wave number, and μ_{ao} and μ'_{so} are respectively the homogeneous absorption and reduced scattering coefficients of the medium. In heterogeneous media, the total DPDW, $U_t(\mathbf{r}_d, \mathbf{r}_s, \omega)$, is a superposition of incident ($U_0(\mathbf{r}_d, \mathbf{r}_s, \omega)$) and scattered ($U_1(\mathbf{r}_d, \mathbf{r}_s, \omega)$) DPDW's. To the first order in the variation of optical absorption and reduced scattering coefficients, the scattered wave is

$$U_1(\mathbf{r}_d, \mathbf{r}_s, \omega) = \int_V T(\mathbf{r}, U_0(\mathbf{r}, \mathbf{r}_s, \omega)) G(|\mathbf{r}_d - \mathbf{r}|) d^3r. \quad (1)$$

Here $G(|\mathbf{r}_d - \mathbf{r}|) = \exp(ik_0|\mathbf{r} - \mathbf{r}_s|) / (4\pi|\mathbf{r} - \mathbf{r}_s|)$ is the Green's function for the DPDW in the homogeneous medium. We call $T(\mathbf{r}, U_0(\mathbf{r}, \mathbf{r}_s, \omega))$ the inhomogeneity function. $T_{abs}(\mathbf{r}, U_0(\mathbf{r}, \mathbf{r}_s, \omega)) = (-\delta\mu_a(\mathbf{r}) v / D_0) U_0(\mathbf{r}, \mathbf{r}_s, \omega)$ for absorbing objects, and $T_{scatt}(\mathbf{r}, U_0(\mathbf{r}, \mathbf{r}_s, \omega)) = (\delta\mu'_s(\mathbf{r}) 3D_0 k_0^2 / v) U_0(\mathbf{r}, \mathbf{r}_s, \omega) - \nabla \ln(\delta\mu'_s + \mu'_{so}) \cdot \nabla U_0(\mathbf{r}, \mathbf{r}_s, \omega)$ for scattering objects. The integral is over the sample volume V .

In this paper, we consider a parallel-plane geometry as shown in Fig.1(a) (which is potentially applicable to the compressed breast geometry). For this case, a natural basis set for the Green's function in Eq.(1) is the simple Weyl expansion form in terms of spatial frequencies p, q, m [10], i.e.

$$G(|\mathbf{r}_d - \mathbf{r}|) = \frac{i}{8\pi^2} \int \int_{-\infty}^{\infty} \frac{dp dq}{m} \exp[ip(x_d - x) + iq(y_d - y) + im(z_d - z)] , \quad (2)$$

where we assume $z_d > z$ without losing generality. $m = (k_0^2 - p^2 - q^2)^{\frac{1}{2}}$ with $\text{Im}(m) > 0$. Using Eq.(2) and taking the 2-D spatial Fourier transform of both sides of Eq.(1) (with respect to transverse (x, y) coordinates), we obtain the following relation

$$\tilde{U}_1(p, q, z_d, \mathbf{r}_s, \omega) = \frac{i}{2m} \int_{z_s}^{z_d} \tilde{T}(p, q, z, \mathbf{r}_s, \omega) \exp[im(z_d - z)] dz . \quad (3)$$

The left hand side of Eq.(3) is the 2-D Fourier transform of the scattered DPDW measured on the detection plane $z = z_d$. This integral equation is approximated by a summation

$$\sum_{j=1}^N \tilde{T}(p, q, z_j, \mathbf{r}_s, \omega) \exp(-imz_j) = \frac{2m}{i \delta z} \exp(-imz_d) \tilde{U}_1(p, q, z_d, \mathbf{r}_s, \omega) , \quad (4)$$

where δz is the discretized step size and N is the total number of slices in the z direction.

For the projection image, we replace z_j on the left hand side of Eq.(4) with the estimated slice position of the object. We drop the sum over all *other* z_j 's and then perform a 2-D inverse Fourier transform of \tilde{T} to obtain the projection image. When the object thickness is of order of several transport mean free paths ($1/(\mu_a + \mu'_s)$) we are able to deduce accurately object(s) optical properties. For thicker objects (i.e. > 5 mm), the average over the size of the object weighted by the sum of exponential phase factors reduces the accuracy of the optical properties. However position information is accurate, and the relative optical properties of multiple objects are also very accurate.

To demonstrate the feasibility of this algorithm, we have performed amplitude and phase measurements in a parallel-plane geometry (Fig.1(a)). The experimental setup is shown in Fig.1(b). The system consists of an RF modulated (100 MHz), low power (~ 3 mW) diode laser operating at 786 nm. The source light is fiber guided into a large fish tank of 50L

0.75% Intralipid ($\mu_a=0.03 \text{ cm}^{-1}$, $\mu'_s=8.0 \text{ cm}^{-1}$) enabling the use of infinite medium boundary conditions. A detection fiber couples the detected diffusive wave to a fast avalanche photodiode (APD). A single-side-band (SSB) demodulator is used to homodyne the signal and the reference wave at 100 MHz. The dynamic range of our current setup is ~ 2500 . The source and detection fiber optics are moved by automated stepper motors. The system is very stable for ~ 3 hours.

The experimental geometry is shown in Fig.1(a). The source position was fixed and taken to be the origin of our coordinate system. As shown in Fig.1(a), we “made” the detection plane by scanning a single detection fiber over a square region from $(-4.65, -4.65, 5.0)$ cm to $(4.65, 4.65, 5.0)$ cm in a plane at $z_d=5.0$ cm in steps of size $\Delta x=\Delta y=0.3$ cm. The amplitude and phase of the DPDW were recorded at each position for a total of 1024 points. We directly measured the amplitude and phase in the *homogeneous* medium to obtain $U_0(\mathbf{r}_d, \mathbf{r}_s, \omega)$.

Two absorbing slices each of dimension $1.5 \times 1.5 \times 0.4 \text{ cm}^3$ were then submerged in the turbid medium (0.75% Intralipid). The slices were made of resin plus TiO_2 and absorbing dye. Slice 1 with $\mu_{a1} = 0.20 \text{ cm}^{-1}$ was placed at position $(-1.6, -0.3, 3.0)$ cm and slice 2 with $\mu_{a2} = 0.10 \text{ cm}^{-1}$ was placed at $(1.6, 0.3, 3.0)$ cm. The scattering coefficients of these two slices are the same as background, e.g., 8.0 cm^{-1} . The scattered wave $U_1(\mathbf{r}_d, \mathbf{r}_s, \omega)$ was obtained by subtracting the homogeneous background DPDW $U_0(\mathbf{r}_d, \mathbf{r}_s, \omega)$ from the measured signal $U_t(\mathbf{r}_d, \mathbf{r}_s, \omega)$. The 2-D Fourier transform of $U_1(\mathbf{r}_d, \mathbf{r}_s, \omega)$ leads to the inhomogeneity function $T(p, q, z_j, \mathbf{r}_s, \omega)$ in Eq.(4). In this paper, we use *a priori* information about the object position(s) in z -direction to select a single image slice. e.g., a slice at $z=z_{obj}$ where the inhomogeneity function is $T(p, q, z_{obj}, \mathbf{r}_s, \omega)$. The 2-D inverse Fourier transform of $T(p, q, z_{obj}, \mathbf{r}_s, \omega)$ gives an accurate spatial map of the absorption variations $\delta\mu_a(x, y, z_{obj})$.

The reconstructed images from experimental data are shown in Fig.(2). The two objects are well resolved (with a peak-to-trough of >2). The reconstructed x - y positions of these two slices are about $(-1.80, -0.25)$ cm and $(1.85, 0.25)$ cm, close to their true x - y positions $(-1.6, -0.3)$ cm and $(1.6, 0.3)$ cm. Inaccuracies in the position measurements might account for the

discrepancy. Images shown in Fig.(2 (b-c)) are unprocessed. The reconstructed absorption coefficients are well above the background noise level and close to the true values (e.g., $\mu_{a1}^{rec} \approx (0.22 \pm 0.03) \text{ cm}^{-1}$) and $\mu_{a2}^{rec} \approx (0.13 \pm 0.03) \text{ cm}^{-1}$. The noise in the reconstruction is mainly from the finite step size and scan region, the positional error and the electronics. The refractive index mismatch between the object and background medium also contributes to the inaccuracy in the reconstructed optical properties. The FFT calculation takes less than 200 msec CPU time on Sun Sparc10 workstation and the presence of multiple objects does not increase the computation complexity.

The feasibility of FFT algorithm for imaging scattering object has also been demonstrated. The geometry is the same as in Fig.1 (a). In this case we used spherical objects as heterogeneities instead of thin slices to test how accurate our algorithm is for imaging extended objects. Sphere 1 of radius 0.75 cm with $\mu'_{s1} \approx 16 \text{ cm}^{-1}$ was placed at (-1.6, -0.3, 3.0) cm, sphere 2 of the same radius with $\mu'_{s2} \approx 26 \text{ cm}^{-1}$ was placed at (1.6, 0.3, 3.0) cm. Both spheres have the same absorption coefficient as the background, e.g., 0.02 cm^{-1} . We see from Fig.3 that positional information about these two scattering objects is recovered. In this case, we use a slice through the sphere center at $z=z_{obj}$ and obtain 2-D scattering *contrast image*. We do not expect to reconstruct the scattering coefficients accurately since the objects are extended. Notice however that we were still able to obtain the correct positions and we see that the two objects are well resolved (Fig.3). Furthermore, the *ratio* of the reconstructed scattering coefficients is close to the true ratio, .e.g., $\mu'_{s2}{}^{rec} / \mu'_{s1}{}^{rec} \approx 1.35$ while the true ratio is about 1.62.

Depth information is required to obtain full 3-D images with this diffraction tomography technique. One simple method is to use a secondary localization scheme to deduce object depth. Alternatively two projection images of the sample along orthogonal directions provide sufficient information for 3-D reconstruction.

To conclude, we have successfully applied near field diffraction tomography, diffuse photon density waves, and FFT's to obtain projection images of hidden objects in highly scattering tissue phantom. It may be possible to obtain clinical projection images in real time with

this fast FFT approach. The geometry used so far has been infinite. In practice, boundary effects present important problems. On the one hand, matching materials might be used to reduce the boundary effects. On the other hand, the introduction of a surface integral term in Eq.(1) or better Green functions (which vanish on the extrapolated boundary) may be used to incorporate boundary effects. The technique presented provides a basis for more complicated and realistic reconstruction methods to address these issues.

It is a pleasure to acknowledge useful discussions with Maureen O'Leary. A.G.Y acknowledges support from the NSF under grant No. DMR93-06814. B.C. acknowledges support in part from NIH under grant Nos. CA 50766 and CA 60182.

REFERENCES

- [1] A. Yodh and B. Chance, *Physics Today*, March, 31(1995), and references therein.
- [2] See related studies in Advances in Optical Imaging and Photon Migration, R. Alfano, Ed., (OSA, Orlando, FL, 1996).
- [3] M. Tamura, O. Hazeki, S. Nioka and B. Chance, *Annu. Rev. Physiol.* **51**, 813(1989).
- [4] S. R. Arridge, P. van der Zee, M. Cope and D. T. Delpy, *SPIE Proceedings*, Vol. **1431**, 204(1991); R. L. Barbour, H. L. Graber, Y. Wang, J. H. Chang and R. Aronson, in Medical Optical Tomography: Functional Imaging and Monitoring, G. Müller, Ed., Vol. **IS11**, (SPIE Optical Engineering Press, 1993), p.87; M. A. O'Leary, D. A. Boas, B. Chance and A. G. Yodh, *Opt. Lett.* **20**, 426(1995); C. P. Gonatas, M. Ishii, J. S. Leigh and J. Schotland, *Phys. Rev. E* **52**, 4361(1995); B. M. Pogue, M. S. Patterson, H. Jiang and K. D. Paulsen, *Phys. Med. Biol.* **40**, 1709(1995); H.B. Jiang, K. D. Paulsen, U. L. Osterberg, B. W. Pogue and M. S. Patterson, *Opt. Lett.* **20**, 2128(1995).
- [5] S. Fantini, M. A. Franceschini, G. Gaida, E. Gratton, H. Jess. W. W. Mantulin, K. T. Moesta, P. M. Schlag and M. Kaschke, *Med. Phys.* **23**, 149(1996).
- [6] ART-Algebraic Reconstruction Technique; SIRT-Simultaneous Iterative Reconstruction Technique, see Principles of Computerized Tomographic Imaging by A. C. Kak and M. Slaney, (IEEE Press, 1988) Chapter 7.
- [7] E. Wolf, *Opt. Commun.* **1**, 153(1969); E. Wolf, in Trends in Optics, Anna Consortini, ed., (Academic Press, San Diego, 1996), p.83; J. Devaney, *Inverse Problems* **2**, 161(1986).
- [8] D. N. Pattanayak, *GE Tech. Info. Series* **91CRD241**, 1991; C. L. Matson, N. Clark, L. McMackin and J. S. Fender, in Advances in Optical Imaging and Photon Migration, R. Alfano, Ed., (OSA, Orlando, FL, 1996), p.261(AWD2-1).
- [9] M. S. Patterson, B. Chance and B. C. Wilson, *Appl. Opt.* **28**, 2331-2335(1989).
- [10] A. Baños, Dipole radiation in the presence of a conducting half-space. (Pergamon, New York, 1966) p.18.

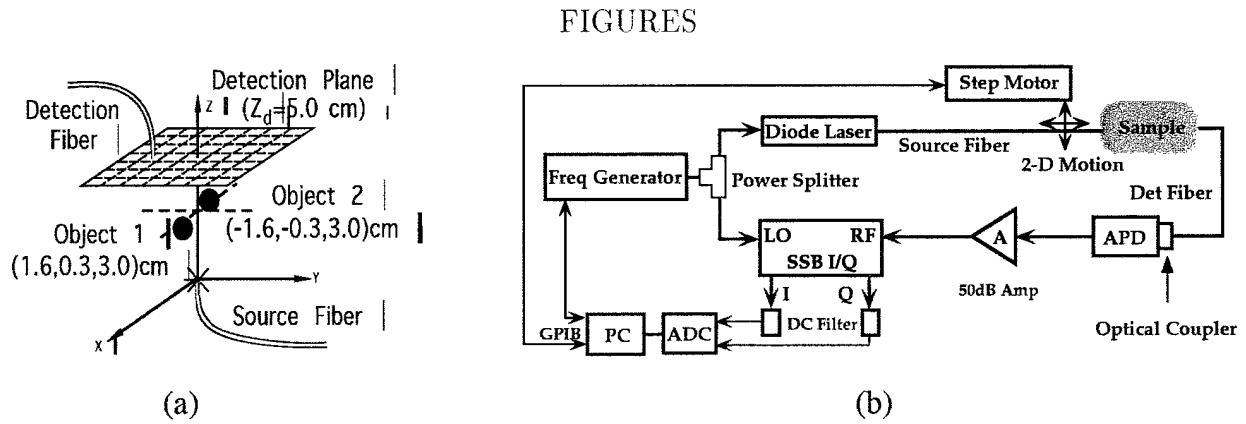


FIG. 1. (a) and (b) illustrate the experimental geometry and setup, respectively. In (a): the source is fixed at the origin and the detector scans in a planar geometry at $z=z_d=5.0$ cm over 9.3×9.3 cm² region. In (b): APD-Avalanche Photo Diode; A-Amplifier; SSB I/Q-Single Side Band In-phase/Quadrature-phase Demodulator; LO-Local Port; RF-Radio Frequency Port; ADC-Analog to Digital Converter; GPIB-General Purpose Interface Bus.

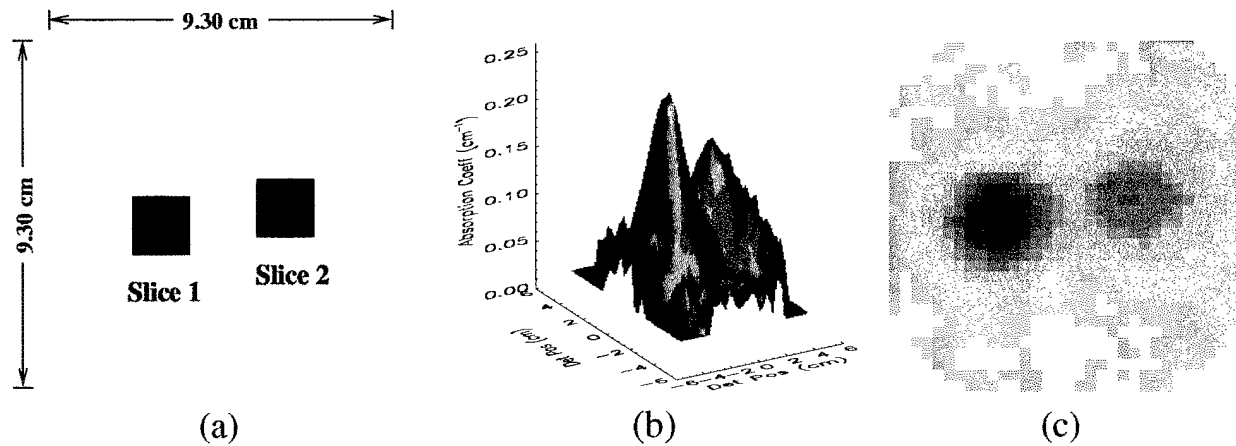


FIG. 2. (a) shows exact positions of the two slices. (b) and (c) illustrate the surface and planar images of two absorbing slices. The absorption coefficients and the positions of the two slices are recovered as shown in (b) and (c).

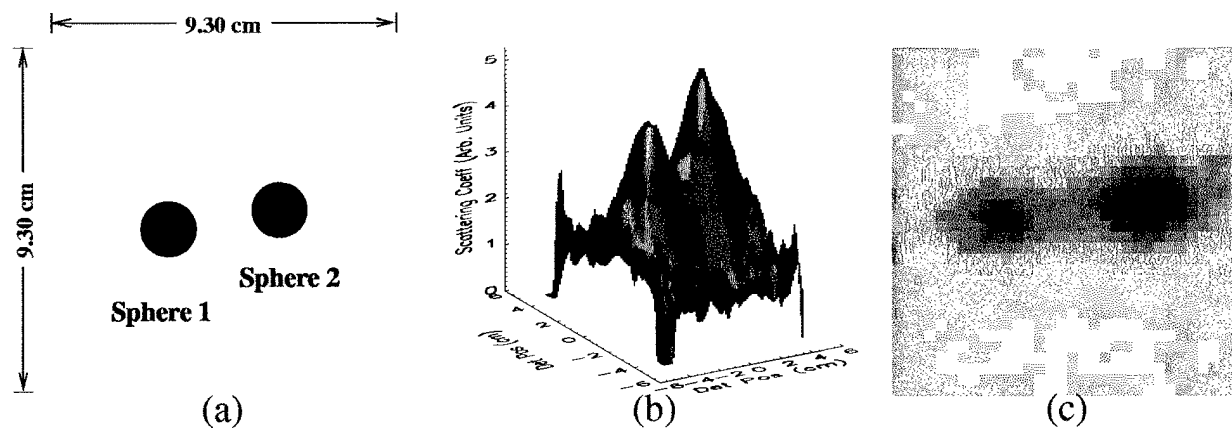


FIG. 3. (a) shows exact positions of the two spheres. (b) and (c) illustrate the surface and planar images of two scattering spheres. The FFT algorithm is sensitive to the scattering properties and the reconstructed ratio of scattering coefficients is close to the true ratio.